# An Implementation of King's Green Functions in Thin Wire Scattering Problems

**Ömer Zor[1] and Burak Polat[2]**

[1] Electronics Engineering Department
Uludağ University, Bursa, TR-16059, Turkey
omerzor@uludag.edu.tr

[2] Electrical and Electronics Engineering Department
Trakya University, Edirne, TR-22030, Turkey
burakpolat@trakya.edu.tr

***Abstract*** ─ We investigate electromagnetic scattering from metallic thin wire structures located over planar and spherical lossy dielectric half-spaces by applying Green's function formulation and method of moments in the resonance region and under "high contrast approximation" (HCA). For this purpose, in the calculations of the impedance matrix and the potential column of the moment system, we employ the Green functions of King valid for arbitrary range under HCA and the asymptotic (far field) Green functions for planar and spherical impedance surfaces delivered by Norton and Wait, respectively. For a verification of the developed codes, the current distributions obtained under plane wave illumination on the arms of a cross shaped thin wire structure are compared to the same results obtained by the commercial software SNEC™. Various illustrations for the scattered electrical field from a thin wire plate located over planar and spherical half-spaces are also presented.

***Index Terms*** ─ Electromagnetic scattering, method of moments, Sommerfeld problem, thin wires.

## I. INTRODUCTION

Ever since the pioneering work [1] by Sommerfeld over a century ago the interest in the derivation of computationally efficient solutions for the radiation fields of a Hertzian dipole in inhomogeneous media has constantly grown in parallel to their applications in diverse areas of electrical engineering. While it is impossible to provide a satisfactory list of all such attempts in literature to date, a wide account can be reached in [2]. The class of solutions to the Sommerfeld problem that constitute the topic of the present investigation is the Green functions derived by King in 1982 [3] for Hertzian dipoles radiating over a planar lossy dielectric half-space. The most distinctive aspect of King's fully analytical solutions, which have been collected in [4] for various different properties of ambient medium, is that they apply for arbitrary range under high contrast approximation (HCA). Following 1999 to date, King's method has been applied to many new geometries involving stratified spherical grounds in numerous works [5-17] initiated by his co-workers.

The thin wire mesh electromagnetic model of an arbitrarily shaped conducting body was first introduced and tested experimentally in 1966 by Richmond [18]. This pioneering work was followed by numerous theoretical as well as experimental investigations [19-27] to specify the ranges of validity of wire mesh models for certain canonical structures. Following the development of the method of moments (MoM) in 1967 by Harrington [28], there has appeared many papers through the 70's on the MoM formulation of scattering problems for the wire mesh structures over a dielectric half-space due to their importance in radar applications [29] Since a computationally efficient analytical solution of the Sommerfeld problem was not available until 1982 [3], in such

*Submitted On: July 4, 2011*
*Accepted On: October 15, 2011*

works the surface wave components of Green functions were generally ignored (as called "reflection coefficient method") for a practical computation of the impedance matrix without estimating the relative error. This gap was then filled by the famous open software NEC-2 [30], which was developed in 1981 in Lawrence Livermore National Laboratory, CA with extensive numerical/asymptotic libraries.

In the present work, we provide the analytical backbone of a software which incorporates the Green functions of King alternative to a similar role of the extensive numerical/asymptotic libraries of NEC-2 whenever HCA applies. While the developed codes equally have the ability to read NEC-2 formatted input files, their main advantage lies in the capability to evolve by proper substitutions of Green functions to take into account various terrain features in any scenario. Accordingly, in Section 2 we provide the MoM formulation of the scattering problem, while the details of the calculation of the elements of the impedance matrix are presented in Section 3. In Section 4 the elements of the potential column in MoM formulation are provided for three different scenarios of propagation over planar and spherical impedance surfaces, and their numerical implementations are presented in Section 5. For a verification of the developed codes we provide the amplitude and phase distributions of currents on the arms of a crossed wire over a planar lossy ground with reference to the same results obtained by the commercial software SNEC™ [31].

A time convention $\exp(-i\omega t)$ is assumed and suppressed.

## II. FORMULATION

Let regions I ( $z>0$ ) and II ( $z<0$ ) be free-space and a simple lossy dielectric with constitutive parameters and wave numbers given as $(\varepsilon_0,\mu_0)$, $k_1=\omega\sqrt{\mu_0\varepsilon_0}$ and $(\varepsilon_2,\mu_0,\sigma_2)$, $k_2=\omega\sqrt{\mu_0(\varepsilon_2+i\sigma_2/\omega)}$, respectively. The complex refractivity of ground is defined by $N=k_2/k_1=\sqrt{\varepsilon_r+i\sigma_2/(\omega\varepsilon_0)}$ with $\varepsilon_r=\varepsilon_2/\varepsilon_0$. The HCA is defined as $|N|^2>>1$ (or equivalently $|N|\geq 3$). Analytically, the lowest value that $|N|$ can take in any simple medium is limited by $\sqrt{\varepsilon_r}$. Therefore, in any medium with $\varepsilon_r\geq 9$ (especially seawater with $\varepsilon_r\approx 75-80$), it can always be satisfied regardless of conductivity and the operating frequency.

Under HCA, the King formulation of Green functions for a Hertzian dipole located at $\vec{r}'=(x',y',z')$ and calculated at $\vec{r}=(x,y,z)$ constitutes "direct" ( $d$ ), "perfect image" ( $i$ ), and "surface wave" ( $s$ ) components, which can be represented in tensorial form by

$$\overline{\overline{G}}(\vec{r},\vec{r}')=\overline{\overline{G}}^{d}(\vec{r},\vec{r}')+\overline{\overline{G}}^{i}(\vec{r},\vec{r}')+\overline{\overline{G}}^{s}(\vec{r},\vec{r}'),$$

$$\begin{aligned}\overline{\overline{G}}^{(d,i,s)} &= \hat{x}\hat{x}g_x^{x(d,i,s)}+\hat{y}\hat{x}g_y^{x(d,i,s)}+\hat{z}\hat{x}g_z^{x(d,i,s)}\\ &+\hat{x}\hat{y}g_x^{y(d,i,s)}+\hat{y}\hat{y}g_y^{y(d,i,s)}+\hat{z}\hat{y}g_z^{y(d,i,s)}\\ &+\hat{x}\hat{z}g_x^{z(d,i,s)}+\hat{y}\hat{z}g_y^{z(d,i,s)}+\hat{z}\hat{z}g_z^{z(d,i,s)}\ .\end{aligned}$$

Here, $g_b^a$ stands for the total $b$-axis electrical field component of the Hertzian dipole with unit moment directed along $a$-axis. The entire set is given for $z,z'>0$ as follows:

$$\begin{aligned}g_x^x &= \frac{e^{ik_1R_1}}{4\pi R_1}\left[\xi_1-\frac{(x-x')^2}{R_1^2}\xi_2\right]\\ &-\frac{e^{ik_1R_2}}{4\pi R_2}\left[\eta_1-\frac{(x-x')^2}{R_2^2}\eta_2\right]\\ &+\frac{e^{ik_1R_2}}{2\pi R_2}\frac{1}{N}\left\{\frac{z+z'}{R_2}\eta_3-\frac{\eta_1}{N}+\frac{(y-y')^2}{R_2^2}\frac{\eta_2}{N}\right.\\ &\left.-\frac{\Xi}{N^2}\frac{R_2}{P^3}\left[ik_1R_2(x-x')^2+\frac{R_2^2}{P^2}(y-y')^2\right]\right\},\end{aligned}$$

$$\begin{aligned}g_y^x &= -\frac{(x-x')(y-y')}{R_1^2}\frac{e^{ik_1R_1}}{4\pi R_1}\xi_2\\ &+\frac{(x-x')(y-y')}{R_2^2}\frac{e^{ik_1R_2}}{4\pi R_2}\eta_2\\ &-\frac{(x-x')(y-y')}{R_2^2}\frac{e^{ik_1R_2}}{2\pi R_2}\\ &\times\frac{\Xi}{N^2}\left[\eta_2+\frac{1}{N}\frac{R_2^3}{P^3}\left(ik_1R_2-\frac{R_2^2}{P^2}\right)\right],\end{aligned}$$

$$g_z^x = -\frac{(x-x')(z-z')}{R_1^2}\frac{e^{ik_1R_1}}{4\pi R_1}\xi_2 + \frac{(x-x')(z+z')}{R_2^2}\frac{e^{ik_1R_2}}{4\pi R_2}\eta_2 - \frac{x-x'}{R_2}\frac{e^{ik_1R_2}}{2\pi R_2}\frac{1}{N}\left[\eta_3 + \frac{\Xi}{N}ik_1R_2\frac{R_2}{P}\right],$$

$$g_x^y = g_y^x ,$$

$$g_y^y = \frac{e^{ik_1R_1}}{4\pi R_1}\left[\xi_1 - \frac{(y-y')^2}{R_1^2}\xi_2\right] - \frac{e^{ik_1R_2}}{4\pi R_2}\left[\eta_1 - \frac{(y-y')^2}{R_2^2}\eta_2\right] + \frac{e^{ik_1R_2}}{2\pi R_2}\frac{1}{N}\left\{\begin{array}{l}\frac{z+z'}{R_2}\eta_3 - \frac{\eta_1}{N} \\ +\frac{\eta_2}{N}\frac{(x-x')^2}{R_2^2} - \frac{\Xi}{N^2}\frac{R_2}{P^3} \\ \times\left[ik_1R_2(y-y')^2 + \frac{R_2^2}{P^2}(x-x')^2\right]\end{array}\right\},$$

$$g_z^y = -\frac{(y-y')(z-z')}{R_1^2}\frac{e^{ik_1R_1}}{4\pi R_1}\xi_2 + \frac{(y-y')(z+z')}{R_2^2}\frac{e^{ik_1R_2}}{4\pi R_2}\eta_2 - \frac{y-y'}{R_2}\frac{e^{ik_1R_2}}{2\pi R_2}\frac{1}{N}\left[\eta_3 + \frac{\Xi}{N}ik_1R_2\frac{R_2}{P}\right],$$

$$g_x^z = -\frac{(x-x')(z-z')}{R_1^2}\frac{e^{ik_1R_1}}{4\pi R_1}\xi_2 - \frac{(x-x')(z+z')}{R_2^2}\frac{e^{ik_1R_2}}{4\pi R_2}\eta_2 + \frac{x-x'}{R_2}\frac{e^{ik_1R_2}}{2\pi R_2}\frac{1}{N}\left[\eta_3 + \frac{\Xi}{N}ik_1R_2\frac{R_2}{P}\right],$$

$$g_z^z = -\frac{(y-y')(z-z')}{R_1^2}\frac{e^{ik_1R_1}}{4\pi R_1}\xi_2 - \frac{(y-y')(z+z')}{R_2^2}\frac{e^{ik_1R_2}}{4\pi R_2}\eta_2 + \frac{y-y'}{R_2}\frac{e^{ik_1R_2}}{2\pi R_2}\frac{1}{N}\left[\eta_3 + \frac{\Xi}{N}ik_1R_2\frac{R_2}{P}\right],$$

$$g_z^z = \frac{e^{ik_1R_1}}{4\pi R_1}\left[\xi_1 - \frac{(z-z')^2}{R_1^2}\xi_2\right] + \frac{e^{ik_1R_2}}{4\pi R_2}\left[\eta_1 - \frac{(z+z')^2}{R_2^2}\eta_2\right] + \frac{\Xi}{N}ik_1P\frac{e^{ik_1R_2}}{2\pi R_2},$$

with

$$R_{1,2}(\vec{r},\vec{r}') = \left|\vec{r} \mp \vec{r}'\right| = \left[(x-x')^2 + (y-y')^2 + (z \mp z')^2\right]^{1/2},$$

$$P = \left[(x-x')^2 + (y-y')^2\right]^{1/2},$$

$$U = \frac{k_1R_2}{2N^2}\left[\frac{R_2 + N(z+z')}{P}\right]^2,$$

and the dimensionless parameters

$$\xi_1 = 1 - \frac{1}{ik_1R_1} - \frac{1}{k_1^2R_1^2}\ ,\ \xi_2 = 1 - \frac{3}{ik_1R_1} - \frac{3}{k_1^2R_1^2}\ ,$$

$$\eta_1 = 1 - \frac{1}{ik_1R_2} - \frac{1}{k_1^2R_2^2}\ ,\ \eta_2 = 1 - \frac{3}{ik_1R_2} - \frac{3}{k_1^2R_2^2},$$

$$\eta_3 = 1 - \frac{1}{ik_1R_2}\ ,\ \Xi = \left(\frac{\pi}{k_1R_2}\right)^{1/2} e^{-iU}F(U)\ ,$$

where

$$F(U) = 1 + i(\pi U)^{1/2}e^{-U}erfc(-iU^{1/2}),$$

is known as the Norton attenuation function. The surface wave components vanish in the limit $|N| \to \infty$.

In thin wire approximation, we assume the wire mesh structure comprises cylindrical segments with fixed length $\ell << \lambda$ and radius $a << \ell$, where $\lambda$ is the wavelength in the ambient medium, as depicted in Fig. 1.

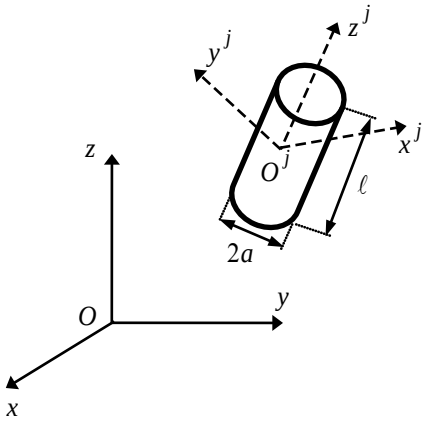


Fig. 1. *j-th* thin wire segment with outer and local reference systems.

In virtue of our choice of pulse basis functions in MoM formulation, we may assume the *j-th* thin wire segment supports a constant current $I_j$, whose density function can be expressed in the local cylindrical coordinates $O^j\rho^j\phi^j z^j$ through the Dirac delta distribution $\delta$ and the unit step function $H$ as

$$\vec{J}_j(\rho^j,\phi^j,z^j)=\hat{z}^j I_j\frac{\delta(\rho^j-a)}{2\pi a}\times\Big[H(z^j+\ell/2)-H(z^j-\ell/2)\Big].$$

The radiation field of *j-th* segment is given by the volume integral

$$\vec{E}_j(\vec{r})=i\omega\mu_0\int\overline{\overline{G}}(\vec{r};\vec{r}^{\,j'})\cdot\vec{J}_j(\vec{r}^{\,j'})d\vartheta^{j'}=I_j\vec{f}_j(\vec{r}),\quad(1)$$

and the total radiatied field by a total of $M$ segments in a mesh is expressed by

$$\vec{E}(\vec{r})=\sum_{j=1}^{M}\vec{E}_j(\vec{r})=\sum_{j=1}^{M}I_j\vec{f}_j(\vec{r})\ ,$$

based on the principle of superposition. Accordingly, the total electrical field at any point in space reads

$$\vec{E}^{tot}(\vec{r})=\vec{E}^{inc}(\vec{r})+\vec{E}(\vec{r}),$$

where $\vec{E}^{inc}(\vec{r})$ is the total field calculated at any point in the absence of the scatterer. Applying the collocation method, the boundary condition on the segments yields the linear system of equations

$$\sum_{j=1}^{M}Z_{mj}I_j=V_m\ ,\quad m=1,2,...,M\ ,$$

$$Z_{mj}=i\omega\mu_0\int_{-\ell/2}^{\ell/2}\int_{0}^{2\pi}\hat{\ell}_m\cdot\overline{\overline{G}}(\vec{r}_m;\vec{r}^{\,j'})\cdot\hat{z}^{\,j}\Big|_{\rho^{j'}=a}\frac{d\phi^{j'}}{2\pi}dz^{j'}\ ,\quad(2)$$

$$V_m=-\vec{E}^{inc}(\vec{r}_m)\cdot\hat{\ell}_m\ .\quad(3)$$

Here, $\vec{r}_m=(x_m,y_m,z_m)$ denotes the central point and $(x_m^I,y_m^I,z_m^I)$ & $(x_m^{II},y_m^{II},z_m^{II})$, the starting & end points of *m-th* segment in the presumed direction of current flow. Then, its unit tangential vector can be written as

$$\hat{\ell}_m=\ell_{mx}\hat{x}+\ell_{my}\hat{y}+\ell_{mz}\hat{z}=\Big[(x_m^{II}-x_m^I)\hat{x}+(y_m^{II}-y_m^I)\hat{y}+(z_m^{II}-z_m^I)\hat{z}\Big]\Big/\ell,$$

where

$$\ell=\Big[(x_m^{II}-x_m^I)^2+(y_m^{II}-y_m^I)^2+(z_m^{II}-z_m^I)^2\Big]^{1/2},\ \forall m\ .$$

At each junction the corresponding junction condition on currents increases the dimension of the linear system by one. In case of $L$ junctions in a wire mesh, the currents are calculated by multiplying the extended system $[Z]_{(M+L)\times M}\cdot[I]_{M\times1}=[V]_{(M+L)\times1}$ by the Hermitian transpose $[Z]^*_{M\times(M+L)}$ of the extended impedance matrix before inversion as follows:

$$[I]_{M\times1}=\Big([Z]^*_{M\times(M+L)}\cdot[Z]_{(M+L)\times M}\Big)^{-1}\times\Big([Z]^*_{M\times(M+L)}\cdot[V]_{(M+L)\times1}\Big).$$

Alternative models for junctions can be reached at [32-34].

The total radiation (far) field of the wire mesh can be approximated as the superposition of the fields generated by Hertzian dipoles with moment $p_j=I_j\ell$ centered at $\vec{r}=\vec{r}_j$ and directed along $\hat{\ell}_j$ as

$$\vec{E}(\vec{r})=i\omega\mu_0\sum_{j=1}^{M}p_j\overline{\overline{G}}(\vec{r};\vec{r}_j)\cdot\hat{\ell}_j\ .$$

## III. CALCULATION OF THE ELEMENTS OF IMPEDANCE MATRIX

The elements of the impedance matrix comprise three components

$$Z_{mj}=Z_{mj}^d+Z_{mj}^i+Z_{mj}^s\ ,$$

which require to be calculated separately through

$$Z_{mj}^{(d,i,s)} = i\omega\mu_0 \int_{-\ell/2}^{\ell/2} \int_0^{2\pi} \hat{\ell}_m \cdot \overline{\overline{G}}^{(d,i,s)}(\vec{r}_m;\vec{r}^{\,j'}) \cdot \hat{z}^{\,j} \Big|_{\rho^{j'}=a} \frac{d\phi^{j'}}{2\pi} dz^{j'} . \tag{4}$$

Since $Z_{mj}^{d}$ and $Z_{mj}^{i}$ are space wave components, their calculations can be carried out directly in the local reference frame $O^j x^j y^j z^j$. Regarding $Z_{mj}^{d}$, the expressions of the difference vector directed from the central point of $j$-*th* to *m-th* segment in local and outer reference frames are given as

$$\vec{r}^{\,m} = (x^m, y^m, z^m),$$

$$\vec{r}_m - \vec{r}_j = (x_m - x_j, y_m - y_j, z_m - z_j),$$

while they are related by

$$\vec{r}^{\,m} = \overline{\overline{T}}_j \cdot (\vec{r}_m - \vec{r}_j) \quad \text{or} \quad \vec{r}_m - \vec{r}_j = \overline{\overline{T}}_j^{\,TR} \cdot \vec{r}^{\,m},$$

through the Euler transformation matrix $\overline{\overline{T}}_j$

$$\overline{\overline{T}}_j = \begin{bmatrix} \cos\alpha_j \cos\beta_j & \sin\alpha_j \cos\beta_j & -\sin\beta_j \\ -\sin\alpha_j & \cos\alpha_j & 0 \\ \cos\alpha_j \sin\beta_j & \sin\alpha_j \sin\beta_j & \cos\beta_j \end{bmatrix},$$

whose inverse is equal to its transpose: $\overline{\overline{T}}_j^{-1} = \overline{\overline{T}}_j^{\,TR}$. The explicit expressions of the 3-D transformation angles $\alpha_j$ ve $\beta_j$ are as follows:

$$\sin\alpha_j = (y_j^{II} - y_j^I) \Big/ [(x_j^{II} - x_j^I)^2 + (y_j^{II} - y_j^I)^2]^{1/2},$$

$$\cos\alpha_j = (x_j^{II} - x_j^I) \Big/ [(x_j^{II} - x_j^I)^2 + (y_j^{II} - y_j^I)^2]^{1/2},$$

$$\sin\beta_j = [(x_j^{II} - x_j^I)^2 + (y_j^{II} - y_j^I)^2]^{1/2} \Big/ \ell,$$

$$\cos\beta_j = (z_j^{II} - z_j^I) \Big/ \ell .$$

Accordingly, under the thin wire approximation one has

$$R_1^2(\vec{r}^{\,m};\vec{r}^{\,j'}) \cong (x^m)^2 + (y^m)^2 + (z^m)^2 + a^2 - 2z^m z^{j'} + (z^{j'})^2,$$

and the $\hat{z}^j$-directed Green functions read

$$g_{x^j}^{z^j d}(\vec{r}^{\,m},\vec{r}^{\,j'}) = -\frac{(x^m - x^{j'})(z^m - z^{j'})}{R_1^2} \frac{e^{ik_1R_1}}{4\pi R_1} \xi_2, \tag{5}$$

$$g_{y^j}^{z^j d}(\vec{r}^{\,m},\vec{r}^{\,j'}) = -\frac{(y^m - y^{j'})(z^m - z^{j'})}{R_1^2} \frac{e^{ik_1R_1}}{4\pi R_1} \xi_2, \tag{6}$$

$$g_{z^j}^{z^j d}(\vec{r}^{\,m},\vec{r}^{\,j'}) = \frac{e^{ik_1R_1}}{4\pi R_1} \left[ \xi_1 - \frac{(z^m - z^{j'})^2}{R_1^2} \xi_2 \right].$$

Substituting the polar transformations $x^{j'} = a\cos\phi^{j'}$ ve $y^{j'} = a\sin\phi^{j'}$ in (5) and (6), a full period integration in (4) yields the resultant regular integral

$$Z_{mj}^{d} = i\omega\mu_0 \int_{-\ell/2}^{\ell/2} \begin{bmatrix} \ell^{mx} t_{x^j}^{z^j d}(\vec{r}^{\,m},\vec{r}^{\,j'}) \\ +\ell^{my} t_{y^j}^{z^j d}(\vec{r}^{\,m},\vec{r}^{\,j'}) \\ +\ell^{mz} g_{z^j}^{z^j d}(\vec{r}^{\,m},\vec{r}^{\,j'}) \end{bmatrix} dz^{j'},$$

with

$$t_{x^j}^{z^j d}(\vec{r}^{\,m},\vec{r}^{\,j'}) = -\frac{x^m(z^m - z^{j'})}{R_1^2} \frac{e^{ik_1R_1}}{4\pi R_1} \xi_2,$$

$$t_{y^j}^{z^j d}(\vec{r}^{\,m},\vec{r}^{\,j'}) = -\frac{y^m(z^m - z^{j'})}{R_1^2} \frac{e^{ik_1R_1}}{4\pi R_1} \xi_2,$$

$$\hat{\ell}^m = \ell^{mx}\hat{x}^j + \ell^{my}\hat{y}^j + \ell^{mz}\hat{z}^j = \overline{\overline{T}}_j \cdot \hat{\ell}_m,$$

which is a calculated numerically. Similar considerations hold for the calculation of $Z_{mj}^{i}$.

In calculating the surface wave components $Z_{mj}^{s}$, we express the source points in the local reference frame and the observation points in the outer reference frame. For this purpose, we set $\vec{r} = \vec{r}_m$, $\vec{r}' = \vec{r}_j' = \vec{r}_j + \overline{\overline{T}}_j^{\,TR} \cdot \vec{r}^{\,j'}$ in King's Green functions, where $\vec{r}_j' = (x_j', y_j', z_j')$ and $\vec{r}^{\,j'} = (x^{j'}, y^{j'}, z^{j'})$ (see Fig. 2).

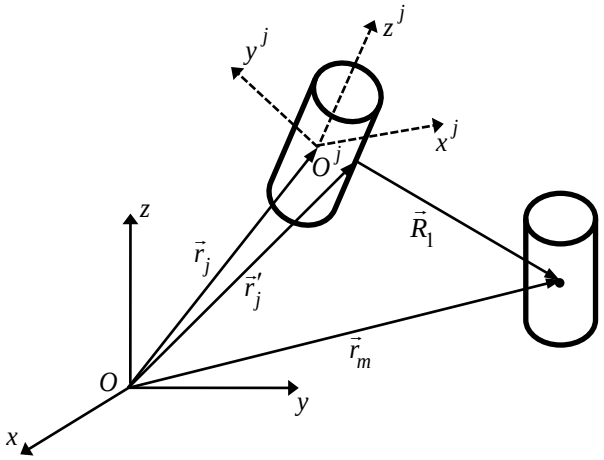


Fig. 2. *j-th* and *m-th* thin wire segments and position vectors.

Under the thin wire approximation one has

$$R_{1,2}^2(\vec{r}_m;\vec{r}^{\,j'}) \cong (x_m - x_j)^2 + (y_m - y_j)^2 + (z_m - z_j)^2 + a^2 + z^{j'2} - 2z^{j'}\begin{bmatrix}(x_m - x_j)\cos\alpha_j \sin\beta_j \\ +(y_m - y_j)\sin\alpha_j \sin\beta_j \\ +(z_m \mp z_j)\cos\beta_j\end{bmatrix},$$

$$P^2 \cong (x_m - x_j)^2 + (y_m - y_j)^2 - 2z^{j'}\sin\beta_j\begin{bmatrix}(x_m - x_j)\cos\alpha_j \\ +(y_m - y_j)\sin\alpha_j\end{bmatrix} + (z^{j'})^2\sin^2\beta_j,$$

$$U \cong \frac{k_1 R_2}{2N^2}\left(\frac{R_2 + NI_z}{P}\right)^2,$$

$$I_z = z_m + z'_j \cong z_m + z_j + z^{j'}\cos\beta_j .$$

By describing the following parameters

$$I_x = \int_0^{2\pi}(x_m - x'_j)\frac{d\phi^{j'}}{2\pi} = x_m - x_j - z^{j'}\cos\alpha_j \sin\beta_j ,$$

$$I_{xx} = \int_0^{2\pi}(x_m - x'_j)^2\frac{d\phi^{j'}}{2\pi} = (x_m - x_j - z^{j'}\cos\alpha_j \sin\beta_j)^2 + (a^2/2)(\cos^2\alpha_j \cos^2\beta_j + \sin^2\alpha_j),$$

$$I_{xy} = \int_0^{2\pi}(x_m - x'_j)(y_m - y'_j)\frac{d\phi^{j'}}{2\pi} = (x_m - x_j - z^{j'}\cos\alpha_j \sin\beta_j) \times (y_m - y_j - z^{j'}\sin\alpha_j \sin\beta_j) - (a^2/2)\sin\alpha_j \cos\alpha_j \sin^2\beta_j ,$$

$$I_y = \int_0^{2\pi}(y_m - y'_j)\frac{d\phi^{j'}}{2\pi} = y_m - y_j - z^{j'}\sin\alpha_j \sin\beta_j,$$

$$I_{yy} = \int_0^{2\pi}(y_m - y'_j)^2\frac{d\phi^{j'}}{2\pi} = (y_m - y_j - z^{j'}\sin\alpha_j \sin\beta_j)^2 + (a^2/2)(\sin^2\alpha_j \cos^2\beta_j + \cos^2\alpha_j),$$

$$t_x^{xs} = \int_0^{2\pi} g_x^{xs}\frac{d\phi^{j'}}{2\pi} = \frac{e^{ik_1R_2}}{2\pi R_2}\frac{1}{N}\begin{bmatrix}\frac{I_z}{R_2}\eta_3 - \frac{\eta_1}{N} + \frac{I_{yy}}{R_2^2}\frac{\eta_2}{N} \\ -\frac{\Xi}{N^2}\frac{R_2}{P^3}\left(ik_1R_2I_{xx} + \frac{R_2^2}{P^2}I_{yy}\right)\end{bmatrix},$$

$$t_y^{xs} = \int_0^{2\pi} g_y^{xs}\frac{d\phi^{j'}}{2\pi} = -\frac{I_{xy}}{R_2^2}\frac{e^{ik_1R_2}}{2\pi R_2}\frac{1}{N^2}\left[\eta_2 + \frac{\Xi}{N}\frac{R_2^3}{P^3}\left(ik_1R_2 - \frac{R_2^2}{P^2}\right)\right],$$

$$t_z^{xs} = \int_0^{2\pi} g_z^{xs}\frac{d\phi^{j'}}{2\pi} = -\frac{I_x}{R_2}\frac{e^{ik_1R_2}}{2\pi R_2}\frac{1}{N} \times\left[\eta_3 + \frac{\Xi}{N}ik_1R_2\frac{R_2}{P}\right],$$

$$t_x^{ys} = t_y^{xs} ,$$

$$t_y^{ys} = \int_0^{2\pi} g_y^{ys}\frac{d\phi^{j'}}{2\pi} = \frac{e^{ik_1R_2}}{2\pi R_2}\frac{1}{N}\begin{bmatrix}\frac{I_z}{R_2}\eta_3 - \frac{\eta_1}{N} + \frac{\eta_2}{N}\frac{I_{xx}}{R_2^2} \\ -\frac{\Xi}{N^2}\frac{R_2}{P^3}\left(ik_1R_2I_{yy} + \frac{R_2^2}{P^2}I_{xx}\right)\end{bmatrix},$$

$$t_z^{ys} = \int_0^{2\pi} g_z^{ys}\frac{d\phi^{j'}}{2\pi} = -\frac{I_y}{R_2}\frac{e^{ik_1R_2}}{2\pi R_2}\frac{1}{N} \times\left[\eta_3 + \frac{\Xi}{N}ik_1R_2\frac{R_2}{P}\right],$$

$$t_x^{zs} = \int_0^{2\pi} g_x^{zs}\frac{d\phi^{j'}}{2\pi} = \frac{I_x}{R_2}\frac{e^{ik_1R_2}}{2\pi R_2}\frac{1}{N}\times\left[\eta_3 + \frac{\Xi}{N}ik_1R_2\frac{R_2}{P}\right],$$

$$t_y^{zs} = \int_0^{2\pi} g_y^{zs}\frac{d\phi^{j'}}{2\pi} = \frac{I_y}{R_2}\frac{e^{ik_1R_2}}{2\pi R_2}\frac{1}{N}\times\left[\eta_3 + \frac{\Xi}{N}ik_1R_2\frac{R_2}{P}\right],$$

$$t_z^{zs} = \int_0^{2\pi} g_z^{zs}\frac{d\phi^{j'}}{2\pi} = \frac{\Xi}{N}ik_1P\frac{e^{ik_1R_2}}{2\pi R_2} ,$$

which emerge from the full period integration of the surface wave components of the Green tensor, one reaches the resultant regular integral

$$Z_{mj}^{s} = i\omega\mu_0 \times \int_{-\ell/2}^{\ell/2} \begin{bmatrix} \ell_{mx} t_x^{xs} z_{jx} + \ell_{mx} t_x^{ys} z_{jy} + \ell_{mx} t_x^{zs} z_{jz} \\ + \ell_{my} t_y^{xs} z_{jx} + \ell_{my} t_y^{ys} z_{jy} + \ell_{my} t_y^{zs} z_{jz} \\ + \ell_{mz} t_z^{xs} z_{jx} + \ell_{mz} t_z^{ys} z_{jy} + \ell_{mz} t_z^{zs} z_{jz} \end{bmatrix} dz^{j'},$$

with $\hat{z}_j = z_{jx}\hat{x} + z_{jy}\hat{y} + z_{jz}\hat{z} = \overline{\overline{T}}_j^{TR} \cdot \hat{z}^j$, which requires to be calculated numerically.

## IV. THREE DIFFERENT SCENARIOS

The influence of the geometrical and physical properties of the ambient medium in scattering phenomenon appears in the expression (3), which is determined by the incident field. In this section, we consider three different scenarios for the incident field and the ambient medium for a numerical investigation.

### A. Scenario I: Homogeneous plane wave incidence and planar ground

Let the electrical field of an incoming homogeneous plane wave in an arbitrary direction $\hat{n}_i$ in region I be given by

$$\vec{E}^i = \hat{e}_i e^{ik_0 \hat{n}_i \cdot \vec{r}}.$$

The normal of the interface is $\hat{n} \equiv \hat{z}$, while the normal of the incidence plane is calculated as $\hat{q} = \hat{n} \times \hat{n}_i$. By use of the identity $\hat{e}_i = \hat{q}(\hat{q} \cdot \hat{e}_i) - \hat{q} \times (\hat{q} \times \hat{e}_i)$ one can decompose the incident wave into TE and TM components as

$$\vec{E}^i = \vec{E}_{TE}^i + \vec{E}_{TM}^i,$$

where

$$\vec{E}_{TE}^i = -\hat{q} \times (\hat{q} \times \hat{e}_i) e^{i\vec{k} \cdot \vec{r}} = (\hat{q} \times \hat{e}_i) \times \hat{q}\, e^{i\vec{k} \cdot \vec{r}},$$

$$\vec{E}_{TM}^i = \hat{q}(\hat{q} \cdot \hat{e}_i) e^{i\vec{k} \cdot \vec{r}},$$

while their reflected components read

$$\vec{E}_{TE}^r = (\hat{q} \times \hat{e}_i) \times \hat{q} \Gamma_{TE} e^{i\vec{k} \cdot \vec{r}}, \vec{E}_{TM}^r = \hat{q}(\hat{q} \cdot \hat{e}_i) \Gamma_{TM} e^{i\vec{k} \cdot \vec{r}},$$

with the Fresnel coefficients

$$\Gamma_{TE} = \frac{N\cos\psi - (N - \sin^2\psi)^{1/2}}{N\cos\psi + (N - \sin^2\psi)^{1/2}},$$

$$\Gamma_{TM} = \frac{\cos\psi - (N - \sin^2\psi)^{1/2}}{\cos\psi + (N - \sin^2\psi)^{1/2}}.$$

Here, $\psi \in [0, \pi/2)$ stands for the angle between the unit vectors $\hat{n}$ and $\hat{n}_i$. Accordingly, the total incident field can be expressed by

$$\vec{E}^{inc} = \vec{E}_{TE}^i + \vec{E}_{TE}^r + \vec{E}_{TM}^i + \vec{E}_{TM}^r.$$

### B. Scenario II: A monopole antenna and planar impedance ground

In virtue of (1), the incident far field of a monople antenna located at $\vec{r} = \vec{r}'$ along $\hat{\ell}_M$ direction with moment $p_M$ can be expressed as

$$\vec{E}^{inc}(\vec{r}) = i\omega\mu_0 p_M \overline{\overline{G}}(\vec{r}; \vec{r}') \cdot \hat{\ell}_M. \qquad (7)$$

The elements of the Green tensor can be specified as the Green functions delivered by Norton [35] under HCA and grazing wave incidence as follows:

$$g_x^x = \frac{e^{ik_1 R_1}}{4\pi R_1}\left[1 - \frac{(x-x')^2}{R_1^2}\right] + \frac{e^{ik_1 R_2}}{4\pi R_2}\left[R_h \frac{(y-y')^2}{P^2} - R_v (x-x')^2 \left(\frac{1}{P^2} - \frac{1}{R_2^2}\right)\right] + \frac{e^{ik_1 R_2}}{4\pi R_2}\left[\begin{array}{l} \dfrac{(y-y')^2}{P^2}(1-R_h)F(q) \\ -\dfrac{(x-x')^2}{P^2}\Delta_N^2 (1-R_v)F(W_N) \end{array}\right],$$

$$g_y^x = -\frac{(x-x')(y-y')}{R_1^2}\frac{e^{ik_1 R_1}}{4\pi R_1} - (x-x')(y-y')\frac{e^{ik_1 R_2}}{4\pi R_2}\left[\frac{R_h}{P^2} + R_v\left(\frac{1}{P^2} - \frac{1}{R_2^2}\right)\right] - \frac{(x-x')(y-y')}{P^2}\frac{e^{ik_1 R_2}}{4\pi R_2} \times \left[(1-R_h)F(q) + \Delta_N^2 (1-R_v)F(W_N)\right],$$

$$g_z^x = -\frac{(x-x')(z-z')}{R_1^2}\frac{e^{ik_1 R_1}}{4\pi R_1} + \frac{(x-x')(z+z')}{R_2^2} R_v \frac{e^{ik_1 R_2}}{4\pi R_2} - \frac{x-x'}{R_2}\Delta_N (1-R_v)F(W_N)\frac{e^{ik_1 R_2}}{4\pi R_2},$$

$$g_x^y = g_y^x,$$

$$g_y^y = \frac{e^{ik_1R_1}}{4\pi R_1}\left[1-\frac{(y-y')^2}{R_1^2}\right] + \frac{e^{ik_1R_2}}{4\pi R_2}\left[\begin{array}{l} R_h\dfrac{(x-x')^2}{P^2} \\ -R_v(y-y')^2\left(\dfrac{1}{P^2}-\dfrac{1}{R_2^2}\right)\end{array}\right] + \frac{e^{ik_1R_2}}{4\pi R_2}\left[\begin{array}{l} \dfrac{(x-x')^2}{P^2}(1-R_h)F(q) \\ -\dfrac{(y-y')^2}{P^2}\Delta_N^2(1-R_v)F(W_N)\end{array}\right],$$

$$g_z^y = -\frac{(y-y')(z-z')}{R_1^2}\frac{e^{ik_1R_1}}{4\pi R_1} + \frac{(y-y')(z+z')}{R_2^2}R_v\frac{e^{ik_1R_2}}{4\pi R_2} - \frac{y-y'}{R_2}\Delta_N(1-R_v)F(W_N)\frac{e^{ik_1R_2}}{4\pi R_2},$$

$$g_x^z = -\frac{(x-x')(z-z')}{R_1^2}\frac{e^{ik_1R_1}}{4\pi R_1} - \frac{(x-x')(z+z')}{R_2^2}R_v\frac{e^{ik_1R_2}}{4\pi R_2} + \frac{x-x'}{R_2}\Delta_N(1-R_v)F(W_N)\frac{e^{ik_1R_2}}{4\pi R_2},$$

$$g_y^z = -\frac{(y-y')(z-z')}{R_1^2}\frac{e^{ik_1R_1}}{4\pi R_1} - \frac{(y-y')(z+z')}{R_2^2}R_v\frac{e^{ik_1R_2}}{4\pi R_2} + \frac{y-y'}{R_2}\Delta_N(1-R_v)F(W_N)\frac{e^{ik_1R_2}}{4\pi R_2},$$

$$g_z^z = \frac{P^2}{R_1^2}\frac{e^{ik_1R_1}}{4\pi R_1} + \frac{P^2}{R_2^2}R_v\frac{e^{ik_1R_2}}{4\pi R_2} + \frac{P^2}{R_2^2}(1-R_v)F(W_N)\frac{e^{ik_1R_2}}{4\pi R_2},$$

In Norton's formulation the ground is modeled by a scalar impedance boundary condition (cf.[36, Sec.1.15]) with normalized surface impedance

$$\Delta_N = (1/N)\left[1-(1/N^2)(P/R_2)^2\right]^{1/2},$$

With respect to free space characteristic impedance $Z_0 = 120\pi$, while the reflection coefficients and ground parameters therein are given as

$$R_v = \frac{z+z'-R_2\Delta_N}{z+z'+R_2\Delta_N}, \quad R_h = \frac{z+z'-R_2\delta_0}{z+z'+R_2\delta_0},$$

$$W_N = \frac{ik_1R_2}{2}\left(\frac{z+z'+R_2\Delta_N}{P}\right),$$

$$\delta_0 = N^2\Delta_N, \quad q = \frac{ik_1R_2}{2}\left(\frac{z+z'+R_2\delta_0}{P}\right).$$

### C. Scenario III: A monopole antenna and spherical impedance ground

In this case, the expression (7) still applies, while the Green functions can be adopted as the set given by Wait 37,38] which are derived based on the Pol and Bremmer theory [39,40]. Accordingly, the $z$, $x$, and $y$ axes of the outer Cartesian coordinates in the vicinity of the scatterer can be coincided respectively with the spherical coordinate curves $r, \theta, \phi$ of the globe, whose origin is the central point as depicted in Fig. 3.

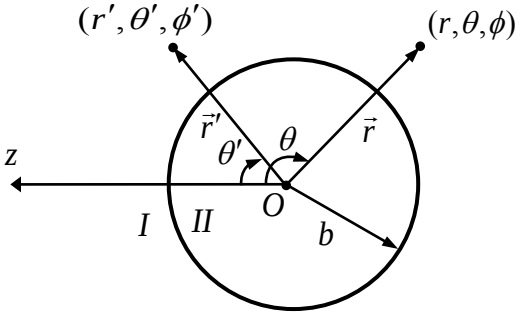


Fig. 3. Spherical earth and its global coordinate system $Or\theta\phi$.

Thereby, the Cartesian tensor components of the Green functions are suitable for our purposes with $\theta' = 0$ can be calculated as

$$g_x^x = e^{i\pi/4}\cos\phi\frac{(\pi A\theta)^{1/2}}{A^2}\frac{e^{ik_1b\theta}}{2\pi b\theta} \times\sum_{s=1}^{\infty}\frac{e^{iA\theta t_s}w'(t_s-y_1)w'(t_s-y_2)}{(t_s-q^2)w^2(t_s)},$$

$$g_y^x = -e^{i\pi/4}\sin\phi(\pi A\theta)^{1/2}\frac{e^{ik_1b\theta}}{2\pi b\theta} \times\sum_{m=1}^{\infty}\frac{e^{iA\theta t_m}w(\bar{t}_m-y_1)w(\bar{t}_m-y_2)}{(\bar{t}_m-q_1^2)w^2(\bar{t}_m)},$$

$$g_z^x = ie^{i\pi/4}\cos\phi\frac{(\pi A\theta)^{1/2}}{A}\frac{e^{ik_1b\theta}}{2\pi b\theta} \times\sum_{s=1}^{\infty}\frac{e^{iA\theta t_s}w'(t_s-y_1)w(t_s-y_2)}{(t_s-q^2)w^2(t_s)},$$

$$g_x^y = e^{i\pi/4}\sin\phi\frac{(\pi A\theta)^{1/2}}{A^2}\frac{e^{ik_1b\theta}}{2\pi b\theta} \times\sum_{s=1}^{\infty}\frac{e^{iA\theta t_s}w'(t_s-y_1)w'(t_s-y_2)}{(t_s-q^2)w^2(t_s)},$$

$$g_y^y = e^{i\pi/4}\cos\phi(\pi A\theta)^{1/2}\frac{e^{ik_1b\theta}}{2\pi b\theta} \times\sum_{m=1}^{\infty}\frac{e^{iA\theta t_m}w(\bar{t}_m-y_1)w(\bar{t}_m-y_2)}{(\bar{t}_m-q_1^2)w^2(\bar{t}_m)},$$

$$g_z^y = ie^{i\pi/4}\sin\phi\frac{(\pi A\theta)^{1/2}}{A}\frac{e^{ik_1b\theta}}{2\pi b\theta} \times\sum_{s=1}^{\infty}\frac{e^{iA\theta t_s}w'(t_s-y_1)w(t_s-y_2)}{(t_s-q^2)w^2(t_s)},$$

$$g_x^z = -ie^{i\pi/4}\frac{(\pi A\theta)^{1/2}}{A}\frac{e^{ik_1b\theta}}{2\pi b\theta} \times\sum_{s=1}^{\infty}\frac{e^{iA\theta t_s}w(t_s-y_1)w'(t_s-y_2)}{(t_s-q^2)w^2(t_s)},$$

$$g_y^z = 0\ ,$$

$$g_z^z = e^{i\pi/4}(\pi A\theta)^{1/2}\frac{e^{ik_1b\theta}}{2\pi b\theta} \times\sum_{s=1}^{\infty}\frac{e^{iA\theta t_s}w(t_s-y_1)w(t_s-y_2)}{(t_s-q^2)w^2(t_s)},$$

where $\Delta=(1/N)\left[1-(1/N^2)\right]^{1/2}$ represents the surface impedance normalized w.r.t. free space characteristic impedance $Z_0=120\pi$; $b=(4/3)\times 6378\ [km]$ is the effective radius of earth taking into account first order tropospheric refractions; $A=(k_1b/2)^{1/3}$, $q=iA\Delta$, and $q_1=N^2q$ are ground constants; $h_1=r'-b$ and $h_2=r-b$ are the heights of the source and observation points above the ground; $y_1=k_1h_1/A$; $y_2=k_1h_2/A$; and $w(t)=\sqrt{\pi}\left[B_i(t)+iA_i(t)\right]$ with $A_i(t)$, $B_i(t)$ denoting standard Airy functions. The Green functions are derived under the natural assumption $h_{1,2}<<b$ and the Rayleigh hypothesis $|\Delta|^2<<1$, which fits well with HCA. The parameters $t_s$ and $\bar{t}_m$ correspond to the discrete complex roots of the Stokes equations $w'(t)-qw(t)=0$ and $w'(t)-q_1w(t)=0$, respectively. They are the eigenvalues of the ground wave modes which are located in the first quadrant of the complex plane and their magnitudes increase with index number. In their determination, we apply the algorithm available in [41, pp. 340-343].

The critical distance, beyond which the influence of the curvature of earth on wave propagation cannot be disregarded, has been determined by Houdzoumis [42] as $\rho_C=b(k_1b/2)^{-1/3}$.

In order to enrich any scenario by including any terrain feature, either land to sea transitions or obstacles ("islands") along the propagation path as devised by Furutsu [43-49] or layered media, it is sufficient to substitute the appropriate set of Green functions into (2) and (3).

The oceanographic parameters such as mean wind speed, fetch length, and wave directionality as described in any sea spectrum [50], [51, pp. 386-403], [52, pp. 109-139], [53-55] can also be taken into account by modifying the normalized surface impedance as $\bar{\Delta}=\Delta+\Delta_{add}$, where the additional term $\Delta_{add}$ was first calculated analytically by Barrick [56] as a 2-D spectral integral involving the sea spectrum using perturbation technique and the Rayleigh hypothesis.

## V. NUMERICAL IMPLEMENTATIONS

In this section, we provide certain numerical results for the three scenarios in Sec. 4 in the frequency range $3-45\,[MHz]$ for propagation over seawater with $\varepsilon_r = 80$, $\sigma = 4\,[S/m]$. First, for a verification of the developed codes we consider the case depicted in Fig. 4 where a crossed wire above planar sea surface is illuminated by a homogeneous plane wave with incidence angle $\psi = 45^\circ$ and unit electrical field amplitude.

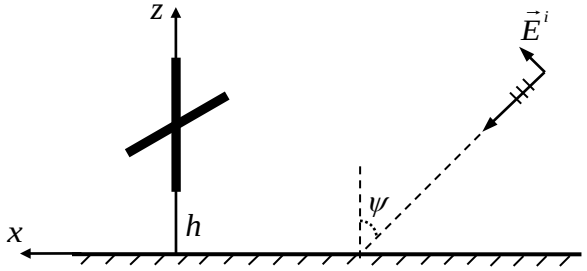


Fig. 4. A crossed wire located above planar sea surface and illuminated by a homogeneous plane wave.

The four arms of the cross are assumed to have the same length $3.33\,[m]$ while the height of the bottom arm from ground is $h = 8\,[m]$. The horizontal arms are assumed to lie along the $y$-axis.

In the first set of illustrations, the operating frequency is taken $f = 3\,[MHz]$ ($\lambda = 100\,[m]$) for which each arm length is $\lambda/30$ and $h = 2\lambda/25$. In virtue of thin wire approximation, the geometrical parameters of the segments are picked as $\ell = 0.5\,[m] = \lambda/200\,[m]$ and $a = 1/40\,[m] = \lambda/4000\,[m] = \ell/20$. They fall into the range in which the values of the computed fields remain insensitive. Under this parameterization, the total number of segments read 27.

In Figs. 5 and 6, we provide the amplitude and phase distributions of currents on the arms of the crossed wire and relative errors calculated by $\%100\,|(\text{SNEC}^{TM} - CODE)/\text{SNEC}^{TM}|$ with reference to the same results obtained by the commercial software SNEC™.

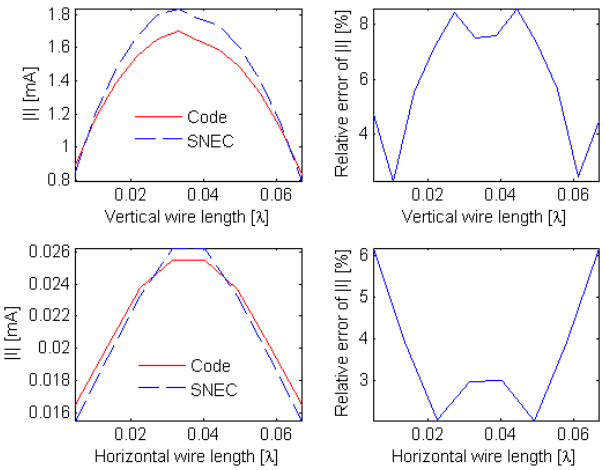


Fig. 5. The amplitude distributions of currents on vertical and horizontal arms and relative errors at $3\,[MHz]$.

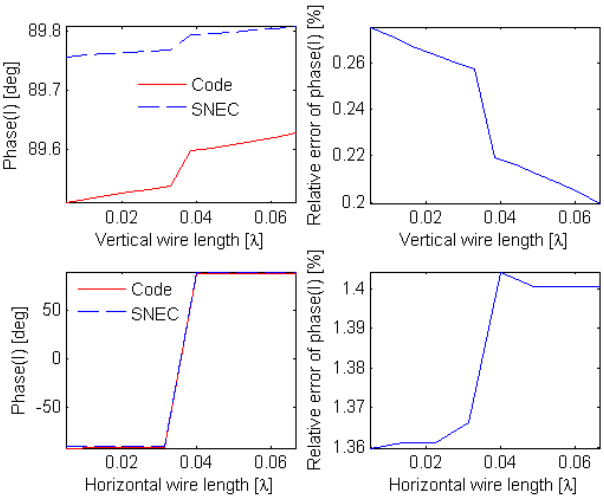


Fig. 6. The phase distributions of currents on vertical and horizontal arms and relative errors at $3\,[MHz]$.

In the second set of illustrations in Figs. 7 and 8, the operating frequency is taken $f = 15\,[MHz]$ ($\lambda = 20\,[m]$) for which the arm length is $\lambda/6$ and $h = 2\lambda/5$, while $\ell = 0.5[m] = \lambda/40\,[m]$ and $a = 1/40\,[m] = \lambda/800\,[m] = \ell/20$.

The relative errors in the two sets of illustrations, which are restricted by $10\%$, stem from the choice of poorly converging pulse basis functions in the MoM scheme, as opposed to the more realistic sinusoidal basis functions employed in SNEC™. It is seen that the error due to theoretical failure of pulse basis functions in satisfying the zero current tip condition reflects on

the entire geometry through matrix inversion in the current calculation.

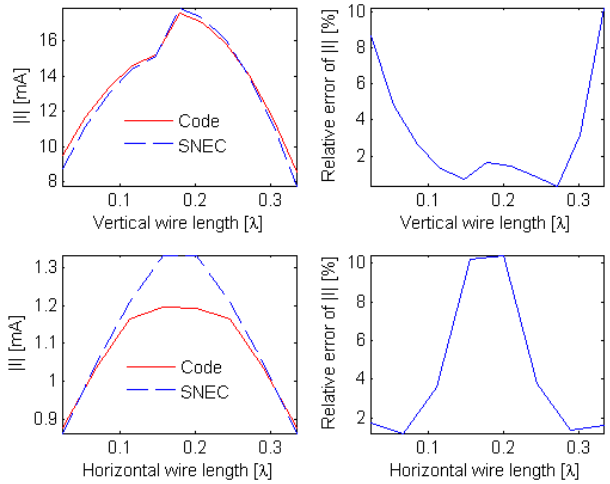


Fig. 7. The amplitude distributions of currents on vertical and horizontal arms and relative errors at $15\,[MHz]$.

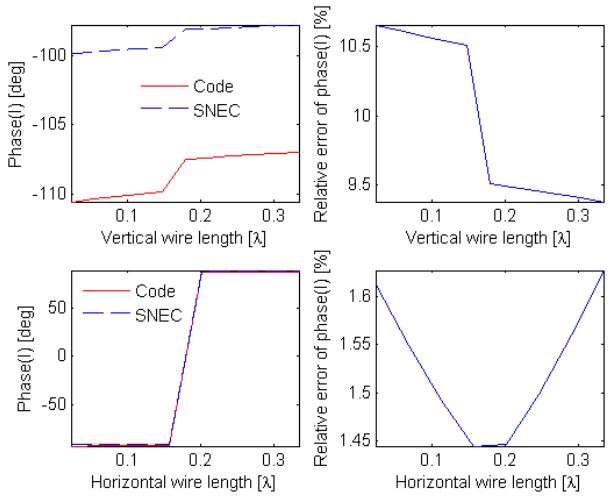


Fig. 8. The phase distributions of currents on vertical and horizontal arms and relative errors at $15\,[MHz]$.

As an application of the second scenario, a wire mesh plate with side length $7\,[m]$ and diagonal length $D \cong 10\,[m]$ is illuminated by a monopole with unit moment at a distance of $10\,[km]$ as depicted in Fig. 9.

In Figs. 10 and 11, we plot the elevation ($Oxz$) and azimuth ($Oxy$) patterns of the total (normalized) scattered field $10\log_{10}(4\pi r^2 |\vec{E}|^2)$ at $15, 30, 45\,[MHz]$ for which the operating wavelength corresponds to $2D, D, 2D/3$, respectively. The symmetries observed in the patterns are due to the symmetric structure of the plate as well as the thin wire approximation that the current flows only along longitudinal direction in every segment.

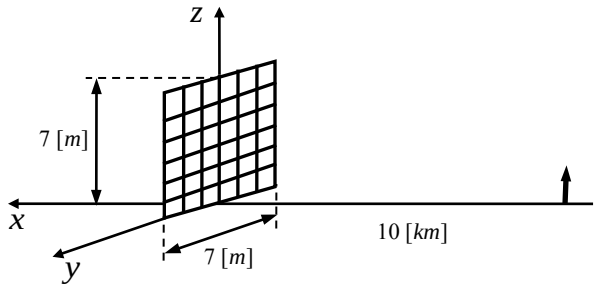


Fig. 9. A wire mesh plate illuminated by a monopole residing on planar sea surface.

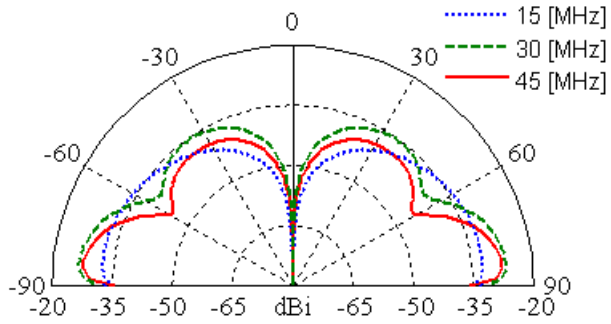


Fig. 10. Elevation patterns for the total scattered field at a) $15$, b) $30$, c) $45\,[MHz]$.

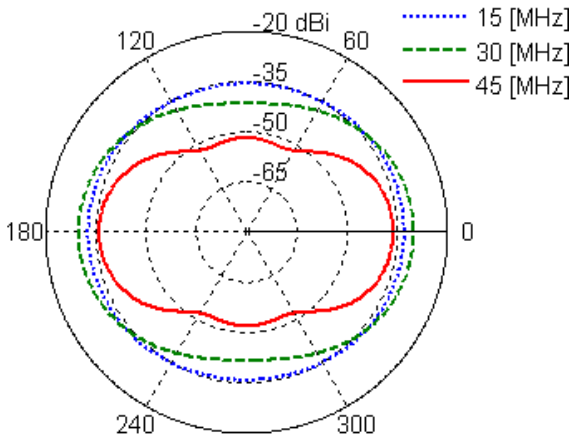


Fig. 11. Azimuth patterns for the total scattered field at a) $15$, b) $30$, c) $45\,[MHz]$.

In Fig. 12, we consider the same scatterer and source as in Fig. 9 on the spherical sea surface illuminated from a distance $10^3\,[km]$.

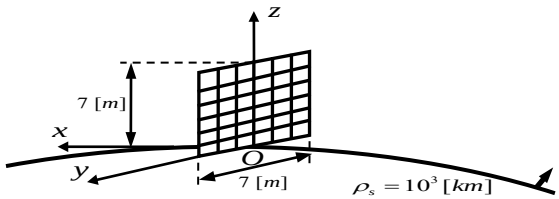


Fig. 12. A wire mesh plate illuminated by a monopole on spherical sea surface.

The total scattered field $20\log_{10}|\vec{E}|$ measured over the sea surface from the origin in the direction of the monopole is plotted in Fig. 13 at $15, 30, 45\,[MHz]$, for which the critical distances are calculated respectively as $77.216\,[km]$, $61.287\,[km]$, $53.539\,[km]$. As expected physically, there is an increased attentuation beyond the critical distances proportional with frequency.

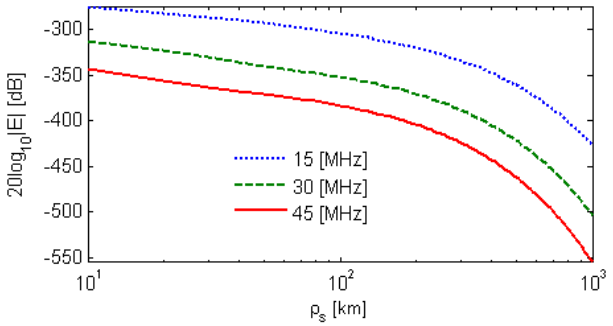


Fig. 13. The total scattered field by a wire mesh plate calculated over sea surface at $15, 30, 45\,[MHz]$.

## VI. CONCLUDING REMARKS

In the present work, we provided a MoM formulation for thin wire structures located over a lossy dielectric ground under HCA employing King's range independent Green functions. Since we are focused on the analytical aspects of the formulation in the first place, our choice of pulse basis functions as the simplest option in a MoM scheme has resulted in a predictable and unavoidable relative error in current calculation as compared to the same results by the commercial software SNEC™, which employs (more realistic) sinusoidal pulse basis functions. Since such a deficiency is not associated with the success of the analytical calculations, the relative error can totally be removed by picking the same set of sinusoidal basis functions as in NEC softwares. While the current codes equally have the ability to read NEC-2 formatted input files, they are developed in the MATLAB™ environment with no commercial concern on total computational time at the time being. However, the numerical implementations put it very clearly that an electromagnetic simulation software that incorporates the Green functions of King may not only provide an alternative to the similar role of the extensive numerical/asymptotic libraries of NEC-2 whenever HCA applies (see also [57,58]), but also provides a capability to evolve by proper substitutions of Green functions to take into account various terrain features in any scenario. This is especially important since the physical (antenna) measurements around critical distances over earth have been reported to diverge seriously from those calculated by NEC-3 and NEC-4 while they follow the analytical results derived by King smoothly (see [59, Sec. 1] and the references cited therein). In light of the expertise gained the research is planned to pursue along the following areas of investigation:

i) Replacing the pulse basis functions in MoM scheme with sinusoidal basis functions following reference works as [60] to eliminate the current relative error with reference to NEC based softwares completely;
ii) Providing a time domain analysis ability to investigate the scattering of actual radar wave forms (as in [61-63]) from mesh structures above sea surface;
iii) Extending the impedance matrix for dielectric coated mesh structures for stealth applications. This is managed by reformulating the MoM matrix by describing a first order impedance boundary condition on each wire segment. For an analytical demonstration of the validity of the impedance boundary condition on arbitrarily shaped surfaces one may refer to [64];
iv) Incorporating Green functions of layered and complex media available in literature ([4-17]) for arbitrary range;
v) Investigation of most efficient NEC2 pre-processors (cf.[65]), modeling guidelines (cf.[66,67]), programming platforms and

algorithms to minimize the computational time for integration and linear algebraic operations at the stage of developing a commercial product.

## ACKNOWLEDGMENT

This work is supported by Uludağ University Research Fund Project No. F-2007/37.

### REFERENCES

[1] A. Sommerfeld, "Propagation of Waves in Wireless Telegraphy," *Ann. Phys.*, vol. 28, pp. 665-736, 1909.

[2] Y. R. Samii, R. Mittra and P. Parhami, "Evaluation of Sommerfeld Integrals for Lossy Half-Space Problems," *Electromagnetics*, vol. 1, no. 1, pp. 1-28, 1981.

[3] R. W. P. King, "New Formulas for the Electromagnetic Field of a Vertical Electric Dipole in a Dielectric or Conducting Half-Space Near its Horizontal Interface," *J. Appl. Phys.*, vol. 53, pp. 8476-8472, 1982 (Erratum: vol. 56, pp. 33-66, 1984).

[4] R. W. P. King, M. Owens, and T. T. Wu, *Lateral Electromagnetic Waves: Theory and Applications to Communications, Geophysical Exploration, and Remote Sensing*, Springer Verlag, New York, 1992.

[5] V. A. Houdzoumis, "Vertical Electric Dipole Radiation Over a Sphere: Character of the Waves that Propagate Through the Sphere," *J. Appl. Phys.*, vol. 86, pp. 3939-3942, 1999.

[6] V. A. Houdzoumis, "Two Modes of Wave Propagation Manifested in Vertical Electric Dipole Radiation Over a Sphere," *Radio Science*, vol. 35, no.1, pp. 19-29, 2000.

[7] D. Margetis and T. T. Wu, "Exactly Calculable Field Components of Electric Dipoles in Planar Boundary," *J. Math. Phys.*, vol. 42 (2), pp. 713-745, 2001.

[8] D. Margetis, "Radiation of Horizontal Electric Dipole on Large Dielectric Sphere," *J. Math. Phys.*, vol. 43, pp. 3162-3201, 2002.

[9] K. Li and S. O. Park, "Electromagnetic Field in the Air Generated by a Horizontal Electric Dipole Located in the Spherical Electrically Earth Coated with a Dielectric Layer," *J. Electromagn. Waves Applicat.*, vol. 17, no. 10, pp. 1399-1417, 2003.

[10] W. Y. Pan and H. Q. Zhang, "Electromagnetic Field of a Vertical Electric Dipole on the Spherical Conductor Covered with a Dielectric Layer," *Radio Sci*., vol. 38, no. 3, p. 1061, 2003.

[11] K. Li, S. O. Park, and H. Q. Zhang, "Electromagnetic Field in the Presence of a Three-Layered Spherical Region," *Progress in Electromagnetics Research*, vol. 45, pp. 103–121, 2004.

[12] K. Li, S. O. Park, and H. Q. Zhang, "Electromagnetic Field over the Spherical Earth Coated with n-Layered Dielectric," *Radio Science*, vol. 39, 2004.

[13] H. Q. Zhang, K. Li, and W. Y. Pan, "The Electromagnetic Field of a Vertical Dipole on the Dielectric-Coated Imperfect Conductor," *J. of Electromag. Waves and Appl.*, vol. 18, no. 10, pp. 1305-1320, 2004.

[14] K. Li and Y. L. Lu, "Electromagnetic Field from a Horizontal Electric Dipole in the Spherical Electrically Earth Covered with n-Layered Dielectrics," *Progress In Electromagnetics Research,* vol. 54, pp. 221-244, 2005.

[15] J. P. Mei and K. Li, "Electromagnetic Field from a Horizontal Electric Dipole on the Surface of a High Lossy Dielectric Coated with a Uniaxial Layer," *Progress in Electromagnetics Research*, vol. 73, pp. 71-91, 2007.

[16] T. Fei, L. W. Li, T. S. Yeo, H. L. Wang, and Q. Wu, "A Comparative Study of Radio Wave Propagation Over the Earth Due to a Vertical Electric Dipole," *IEEE Trans. Antennas Propagat.*, vol. 55, no. 10, pp. 2723-2732, 2007.

[17] L. Liang and K. Li, "Radiation from a Vertical Electric Dipole in the Presence of a Three-Layered Region," *IEEE Trans. Antennas Propagat.*, vol. 55, no. 12, pp. 3469-3475, 2007.

[18] J. H. Richmond, "A Wire-Grid Model for Scattering by Conducting Bodies," *IEEE Trans. Antennas Propagat.*, vol. AP-14, no. 6, pp. 782-786, 1966.

[19] J. L. Lin, W. L. Curtis, and M. C. Vincent, "On the Field Distribution of an Aperture," *IEEE Trans. Antennas Propagat.*, vol. AP-22, pp. 467-471, 1974.

[20] K. S. H. Lee, L. Martin, and J. P. Castillo, "Limitations of Wire-Grid Modeling of a Closed Surface," *IEEE Trans. Electromag. Compat.,* vol. 18, no. 3, pp. 123-129, 1976.

[21] A. C. Ludwig, "Wire Grid Modeling of Surface," *IEEE Trans. Antennas Propagat.,* vol. AP-14, no. 9, pp. 1045-1048, 1987.

[22] A. F. Peterson, "Difficulties Encountered when Attempting to Validate Thin Wire Formulations for Linear Dipole Antennas," *Applied Computational Electromagnetic Society (ACES) Journal,* vol. 4, no. 3, pp. 25-40, 1990.

[23] T. H. Hubing and J. F. Kauffman, "Modeling Electrically Small, Thin Surfaces with Wire Grids," *Applied Computational Electromagnetic Society (ACES) Journal*, vol. 5, no. 1, pp. 19-24, 1990.

[24] J. T. Mayhan, "Characteristic Modes and Wire Grid Modeling," *IEEE Trans. Antennas Propagat.*, vol. 38, no. 4, pp. 457-469, 1990.

[25] S. Kashyap, "Wire Grid and Surface Patch Modelling for EMP Interaction," *IEEE and Propagation Society International Symposium*, AP-S, 1990.

[26] R. Paknys, "The Near Field of a Wire Grid Model," *IEEE Trans. Antennas Propagat.,* vol. 39, no. 7, pp. 994-999, 1991.

[27] R. Paknys and L. R. Raschkowan, "Moment Method Surface Patch and Wire Grid Accuracy in the Computation of Near Fields," *Applied Computational Electromagnetic Society (ACES) Journal*, vol. 12, no. 3, pp. 16-25, 1997.

[28] R. F. Harrington, "Moment Methods for Field Problems," *Proc. of the IEEE*, vol. 55, no. 2, pp. 136-149, 1967.

[29] T. K. Sarkar and R. F. Harrington, "Radar Cross Sections of Conducting Bodies over a Lossy Half Space," *Radio Science*, vol. 15, no. 3, pp. 581-585, 1980.

[30] G. J. Burke and A. J. Poggio, "Numerical Electromagnetics Code (NEC)-Method of Moments," *Lawrence Livermore Laboratory*, Jan. 1981.

[31] SuperNec, Poynting Software (Pty) Ltd., South Africa. http://www.supernec.com/

[32] T. T. Crow and T. H. Shumpert, "Electromagnetic Scattering from Configurations of Thin Wire with Multiple Junctions," *Interaction Note 99*, 1972.

[33] R. W. P. King and T. T. Wu, "Analysis of Crossed Wires in a Plane-Wave Field," *Interaction Note 216*, 1975.

[34] A. R. Bretones, A. S. Extrema, R. M. Gómes, and J. F. Callejón, "About the Study in the Time Domain of Junctions Between Thin Wires," *Applied Computational Electromagnetic Society (ACES) Journal,* vol. 6, no. 2, pp. 2-20, 1991.

[35] K. A. Norton, "The Propagation of Radio Waves over the Surface of the Earth and in the Upper Atmosphere," *Proc. IRE*, vol. 25, pp. 1203-1236, 1937.

[36] T. S. M. Maclean and Z. Wu, *Radiowave Propagation over Ground*, Chapman & Hall, 1993.

[37] J. R. Wait, "Radiation from a Vertical Antenna over a Curved Stratified Ground," *J. Res. Natl. Bur. Stand.*, vol. 56D, no. 4, pp. 237-244, 1956.

[38] J. R. Wait, *Electromagnetic Surface Waves*, in Advances in Radio Research, ed. J.A. Saxton, vol. 1, Academic Press, New York, pp. 157-217, 1964.

[39] B. Van Der Pol, "Theory of Reflection of the Light from a Point Source by a Finite Conducting Flat Mirror, with an Application to Radiotelegraphy," *Physica*, vol. 2, pp. 843-853, 1935.

[40] H. Bremmer, T*errestrial Radio Waves*, New York, Elsevier, 1949.

[41] J. Galejs, *Terresterial Propagation of Long Electromagnetic Waves*, Pergamon Press, New York, 1972.

[42] V. A. Houdzoumis, "Scattering of Electromagnetic Missiles-Part I; Vertical Electric Dipole Radiation over Spherical Earth- Part II," Ph.D. Dissertation, Harvard Univ., 1994.

[43] K. Furutsu, "On the Theory of Radio Wave Propagation over Inhomogeneous Earth," *J. Res. Natl. Bur. Stand.,* vol. 67D, no. 1, pp. 39-62, 1963.

[44] K. Furutsu, "On the Statistical Theory of Electromagnetic Waves in a Fluctuating Medium (I)," *J. Res. Natl. Bur. Stand.*, vol. 67D, no. 3, pp. 303-323, 1963.

[45] K. Furutsu, R. E. Wilkerson, and R. F. Hartmann, "Some Numerical Results Based on the Theory of Radio Wave Propagation over Inhomogeneous Earth," *J. Res. Natl. Bur. Stand.*, vol. 68D, no. 7, pp. 827-846, 1964.

[46] K. Furutsu, "Calculated Curves for Groundwave Propagation over Inhomogeneous Earth with Pronounced Topographical Features," *J. Res. Natl. Bur. Stand.*, vol. 69D, no. 7, pp. 1011-1025, 1965.

[47] K. Furutsu and R. E. Wilkerson, "Optical Approximation for Residue Series of Terminal Gain in Radiowave Propagation over Inhomogeneous Earth," *Proc. IEE*, vol. 118, pp. 1197-1202, 1971.

[48] K. Furutsu, "A Systematic Theory of Wave Propagation over Irregular Terrain," *Radio Science*, vol. 17, no. 5, pp. 1037-1050, 1982.

[49] B. Polat, "Ground Wave Attenuation Curves in the Presence of Successive 2-D Islands," *Bulletin of the Technical University of Istanbul (ARI)*, vol. 54, no. 2, pp. 34-39, 2004.

[50] M. K. Ochi, *Ocean Waves – The Stochastic Approach*, Cambridge University Press, 1998.

[51] G. Kinsman, *Wind Waves: Their Generation and Propagation on the Ocean Surface*, Prentice Hall, Englewood Cliffs, New Jersey, 1965.

[52] O. M. Phillips, *Dynamics of the Upper Ocean*, Cambridge University Press, New York, 1966.

[53] W. J. Pierson and L. Moskowitz, "A Proposed Spectral Form for Fully Developed Wind Seas Based on the Similarity Theory of S. A. Kitaigorodski," *J. Geophys. Res.*, vol. 69, pp. 5181-5190, 1964.

[54] D. E. Hasselmann, M. Dunckel, and J. A. Ewing, "Directional Wave Spectra Observed during

JONSWAP 1973," *J. Phys. Oceanogr.*, vol. 10, pp. 1264-1280, 1980.

[55] F. Berizzi and E. Dalle Mese, "Sea-Wave Fractal Spectrum for SAR Remote Sensing," *IEE Proc.-Radar, Sonar Navig.*, vol. 148, no. 2, pp. 56-66, 2001.

[56] D. E. Barrick, "Theory of HF and VHF Propagation Across the Rough Sea: 1, The Effective Surface Impedance for a Slightly Rough Highly Conducting Medium at Grazing Impedance; 2, Application to HF and VHF Propagation Above the Sea," *Radio Science*, vol. 6, no. 5, pp. 517-533, 1971.

[57] M. M. Weiner, "Validation of the Numerical Electromagnetics Code (NEC) for Antenna Wire Elements in Pproximity to Earth," *Applied Computational Electromagnetic Society (ACES) Journal,* vol. 8, no. 2, pp. 44-71, 1993.

[58] D. B. Davidson and H. T. Mouton, "Validation of and Limitations on the Use of NEC-4 for Radiation from Antennas Buried within a Homogeneous Half-Space," *Applied Computational Electromagnetic Society (ACES) Journal,* vol. 13, no. 3, pp. 302–309, 1998.

[59] R. W. P. King, "Electromagnetic Ground Wave Field of Vertical Antennas for Communication at 1 to 30 MHz," *IEEE Trans. Electromag. Compatibility,* vol. 40, no. 4, pp. 337-342, 1998.

[60] E. H. Newman, "Simple Examples of the Method of Moments in Electromagnetics," *IEEE Trans. Education.,* vol. 31, no. 3, pp. 193-200, 1988.

[61] R. W. P. King and T. T. Wu, "The Propagation of a Radar Pulse in Sea Water," *J. Appl. Phys.*, vol. 73, no. 4, pp. 1581-1590, 1993 (Erratum: *J. Appl. Phys.*, vol. 77, no. 7, pp. 3586-3587, 1995.)

[62] R. W. P. King, "The Propagation of a Gaussian Pulse in Sea Water and its Application to Remote Sensing," *IEEE Trans. Geoscience and Remote Sensing*, vol. 31, no. 3, pp. 595-605, 1993.

[63] R. W. P. King, "Propagation of a Low Frequency Rectangular Pulse in Sea Water," *Radio Science*, vol. 28, no. 3, pp. 299-307, 1993.

[64] B. Polat, "Approximate Boundary Conditions on Anisotropic Sheets," *Progress in Electromagnetics Research-B,* vol. 29, pp. 355–392, 2011.

[65] C. F. du Toit and D. B. Davidson, "Wiregrid: a NEC2 Pre-Processor," *Applied Computational Electromagnetic Society (ACES) Journal,* vol. 10, no. 1, pp. 31–39, 1995.

[66] C. W. Trueman and S. J. Kubina, "Verifying Wire-Grid Model Integrity with Program CHECK," *Applied Computational Electromagnetic Society (ACES) Journal*, vol. 5, no. 2, pp. 17–42, 1990.

[67] L. A. Oyekanmi and J. Watkins, "Selecting Wire Radius for Grid/Mesh Models," *Applied Computational Electromagnetic Society (ACES) Journal*, vol. 5, no. 2, pp. 43–57, 1990.

**Ömer Zor** received B.S. and M.S. degrees in Electronics Engineering from Uludağ University in 2003 and 2006, respectively. Currently, he is a Ph.D. student and works as a research assistant at the same university. His research interests are on analytical and computational methods in electromagnetic theory.

**Burak Polat** received the B.S., M.S., and Ph.D. degrees in Electronics and Communications Engineering from Istanbul Technical University, Istanbul, Turkey in 1993, 1995, and 1997, respectively. In 1998, he was awarded the title of Associate Professor by the Council of Higher Education, Turkey. Between 1994-2000, he worked in Gebze Institute of Technology as a research assistant and Istanbul University as an associate professor. In 2000, he was on leave from Istanbul University to join Applied Electromagnetics Group at Electrical and Computer Engineering Department, Clemson University, SC, USA as a visiting researcher. Between 2000-2001, he worked as a postdoctoral research fellow at the Department of Electromagnetic Systems, Technical University of Denmark and between 2001-2003, he was a senior researcher at Marmara Research Center, Turkish Scientific and Technical Research Council, where he served in military electromagnetic simulation projects. Between May 2003 and October 2005, he worked as an Associate Professor at Department of Electronics and Communications Engineering, Istanbul Technical University (ITU) and Co-Director of ITU-Center for Satellite Communications and Remote Sensing. In 2004, he was at Electromagnetic Compatibility Lab., Electrical and Computer Engineering Department, Concordia University, Montreal, Canada on a 3 months sabbatical leave from ITU. Between 2005-2010, he worked as a full professor at Electronics Engineering and Mathematics Departments of Uludağ University, Turkey. Since September 2010, he serves as the Chair of Electrical and Electronics Department, Trakya University, Turkey. He is also an Associate Editor of Selçuk Journal of Applied Mathematics.

Dr. Polat's research interests include analytical, asymptotic and computational methods in electromagnetic theory.